Vertical growth dynamics of biofilms

Pablo Bravo [1,3,✉], Siu Lung Ng [2], Kathryn A. MacGillivray [2,3], Brian K. Hammer [2], and Peter J. Yunker [1,✉]

[1]School of Physics, Georgia Institute of Technology, Atlanta, Georgia, USA; [2]School of Biological Sciences, Georgia Institute of Technology, Atlanta, Georgia, USA; [3]Interdisciplinary program in Quantitative Biosciences, Georgia Institute of Technology, Atlanta, Georgia, USA

During the biofilm life cycle, bacteria attach to a surface then reproduce, forming crowded, growing communities. Many theoretical models of biofilm growth dynamics have been proposed; however, difficulties in accurately measuring biofilm height across relevant time and length scales have prevented testing these models, or their biophysical underpinnings, empirically. Using white light interferometry, we measure the heights of microbial colonies with nanometer precision from inoculation to their final equilibrium height, producing a novel and detailed empirical characterization of vertical growth dynamics. We propose a heuristic model for vertical growth dynamics based on basic biophysical processes inside a biofilm: diffusion and consumption of nutrients, and growth and decay of the colony. This model captures the vertical growth dynamics from short to long time scales (10 minutes to 14 days) of diverse microorganisms, including bacteria and fungi.

Biofilms | Interferometry | Interface | Timelapse
Correspondence: ***pbravo7@gatech.edu, peter.yunker@gatech.edu***

Significance Statement

The primary mode for microbial life is the biofilm. Experimental difficulty in measuring the vertical growth of biofilms has limited our understanding of this fundamental aspect of biofilm physiology. To address this issue, we measure biofilm topographies with nanometer resolution via interferometry. We found that a diverse array of microbes follow identical trends. Biofilms grow exponentially up to a characteristic thickness, consistent with active growth layer theories. Then, biofilm growth rate decreases linearly with height until growth stops. We construct a simple "interface model" based on these empirical observations, which vastly outperforms alternative heuristics. Interferometric measurements of topography thus represent a facile approach to investigating biofilm development, and our heuristic model provides a biophysical framework to quantify it.

Introduction

Biofilms are surface attached microbial communities composed of cells and extracellular polymeric substance (1–3). Biofilms form when a cell attaches to a surface and reproduces, leading to horizontal and vertical expansion. Understanding the dynamics of this expansion, and the processes responsible for them, is fundamental to understanding biofilm development(4–6). Many studies have focused on understanding the horizontal "range expansion," detailing the impact of physical interactions, the environment, inter-strain competitive dynamics, and more(7–15). Conversely, less is known about the vertical growth of biofilms, i.e., growth perpendicular to the surface, despite its importance for determining access to nutrients and oxygen(16, 17). The initial steps of this process (18, 19), as well as some aspects of competitive growth(20–23), have been studied. However, our knowledge of how vertical growth proceeds over short and long time scales is limited. In particular, while growth curves in liquid media have been studied for years building on the works of Jacques Monod(24, 25), and the horizontal expansion of biofilms on agar plates has been studied extensively (26–28), we lack detailed measurements and a heuristic understanding of vertical growth. As biofilms play important roles in microbial ecology and human health(29, 30), elucidating this fundamental aspect of microbial physiology is crucial.

The characterization of microbial topographies is a growing field(31–38), but with limited focus on the temporal dynamics of the colony. The experimental difficulty in measuring biofilm heights with sufficient precision over many different time scales in a non-destructive manner has limited our understanding of this fundamental phenomenon (39). The utility of traditional optical techniques is limited for a variety of reasons, such as the substantial difference in index of refraction between the biofilm and air. Further, fluorescent proteins and dyes are specific or localized, and thus do not necessarily report the true height of a biofilm, which is composed of both cells and extracellular matrix. Fluorescent stains can also bleach over time, making it difficult to continuously image the biofilm and the surface it sits on, which is necessary for assessing height. Thus, we lack a clear empirical picture of how vertical growth dynamics proceed over short and long time scales.

Due to the many relevant biological and physical parameters(8, 40–42) involved in biofilm modeling, many models are complex, with multiple interacting phases inside and outside of the colony. Often, these models will incorporate a quadratic carrying capacity term to capture the qualitative features of vertical growth dynamics that are initially rapid before eventually saturating. However, while the logistic growth curve captures these qualitative features, it is unclear if logistic growth is quantitatively accurate. To address this issue, many multi-phase, spatial models have been developed (11, 27, 43–47), with a smaller subset of these models explicitly addressing vertical growth, or colony thickness (9, 48, 49). Many of these state of the art models are highly accurate, but their reliance on many precisely measured parameters limits the practical and heuristic utility of such models, especially if many different strains are being compared (50–52). Thus, developing a functional and quantitative understanding of vertical biofilm growth with reduced dimensionality would

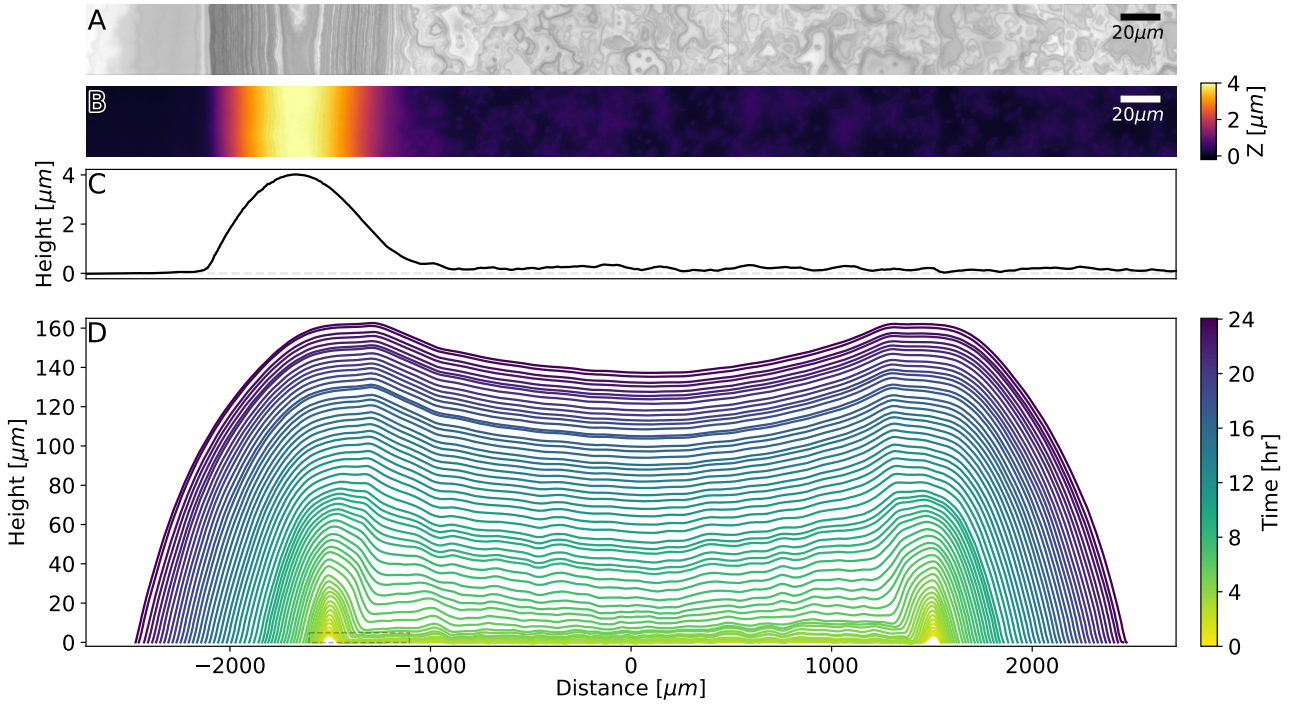

Figure 1. White light interferometry imaging of developing biofilm topography. (A) Light intensity and (B) surface measurement data from the edge of an *Aeromonas veronii* inoculum on LB agar are shown 30 minutes after inoculation. (C) One-dimensional averaged profile of the surface topography is computed from the data in (B). (D) A 24-hour timelapse of averaged profiles from growing *A. veronii* biofilm is shown. The colony expands horizontally (x-axis) and vertically (y-axis), with some of its surface features persisting during development. The scale in the y-axis has been increased to better observe the data. The region shown in panels A-C is marked with a rectangle.

go a long way towards elucidating this fundamental aspect of microbial physiology.

Here, we measure and characterize the vertical growth dynamics of biofilms. Using white light interferometry, we measure biofilm topographies with single nanometer resolution. We perform frequent measurements over 48 hours, and also measure the long time dynamics over two weeks. Guided by our empirical results, we test a simple interface-limited growth model, which accounts for the fact that nutrient diffusion and uptake limit the thickness of the growing zone inside the colony. With just three parameters, this model accurately reproduces the observed asymmetric vertical growth dynamics, and captures steady-state biofilm heights at 14 days.

Results

Using a Zygo Zegage Pro optical profilometer, we measure the growth of multiple microbial colonies, from heights of less than a micrometer after inoculation to hundreds of micrometers after 48 hours of growth (Figure 1A-C). These measurements allow us to reconstruct the interface of a growing microbial colony with high resolution across short and long time scales, both in the lateral (~ 0.2 μm) and vertical direction ($\sim 1.$ nm).

We define colony height h as the mean height in a 2 mm long, 34.6 μm wide strip around the colony center (Figure 1D). Focusing on the center of the colony ensures that we isolate the vertical growth dynamics from the effects of lateral expansion and the initial conditions from inoculation, such as the coffee-ring effect (53, 54). We measured prokaryotic and eukaryotic species, including a wide range of gram-negative and gram-positive bacteria, as well as aerobic and aerotolerant anaerobic yeast (*Saccharomyces cerevisiae*) (see Table S1). All species and strains show similar qualitative behavior; we initially focus on *Aeromonas veronii*, and later expand our study to the full cohort of species and strains.

A. Two-regime growth

We observe that the vertical growth rate (i.e., change in height per unit time) varies over time; initially increasing before reaching a maximum and then slowing down, behavior that is qualitatively replicated by logistic growth (Figure 2A-B). Immediately after inoculation, the vertical growth rate is very low (0-2 μm/hr, Figure 2A inset). This observation is consistent with the fact that cells are adapting to a new environment(55, 56) and that reproduction primarily leads to more horizontal colonization until a monolayer is formed(10).

Plotting Δh as a function of h makes it clear that there are two distinct regimes: (I) a linear increase in vertical growth rate with height for $h \lesssim 27\mu m$ and (II) a linear decrease in vertical growth rate with height for $h \gtrsim 27\mu m$ (Figure 2A-B). The combination of a linear increase and a linear decrease suggests that vertical growth dynamics cannot be governed by a single, unchanging functional relationship between Δh and h. Instead, models of vertical growth must "switch" from one regime to another, and a successful model of this phenomenon must justify this empirical observation. To select such a model, we next look at potential sources of the linear decrease in growth rate of regime (II).

B. Nutrient dynamics in the media

To elucidate the origin of these growth dynamics, we next explore the role of nutrients in the agar. Models of micro-

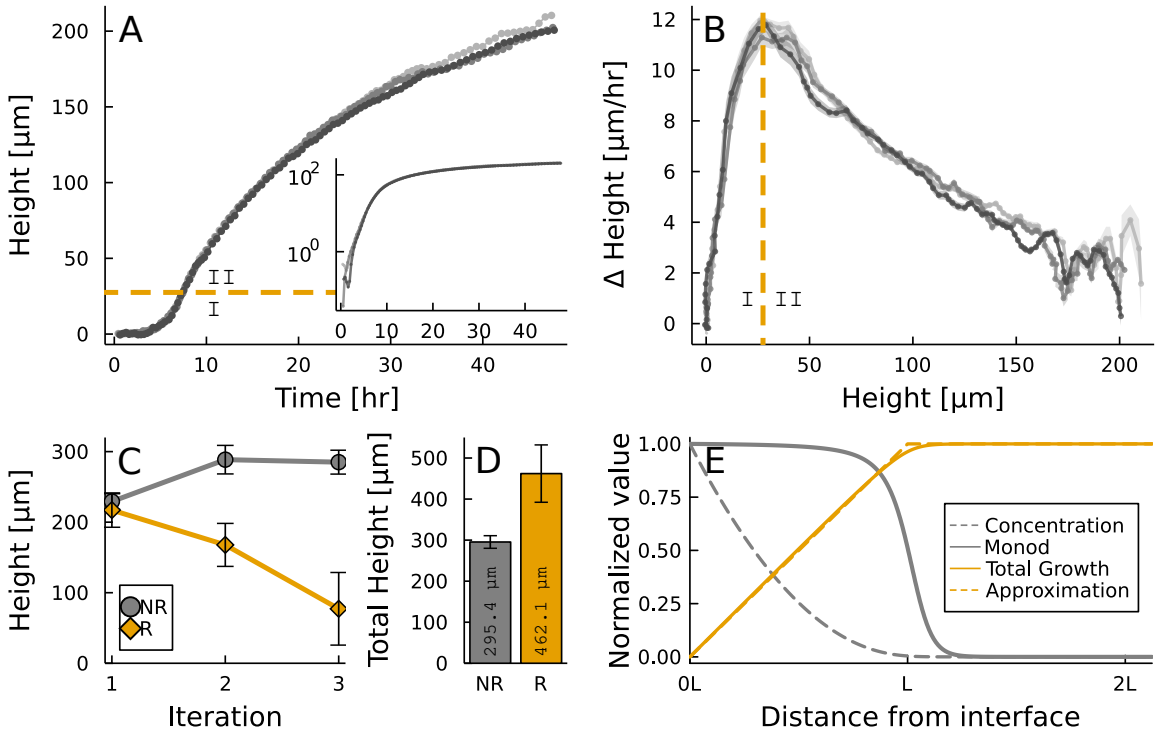

Figure 2. Biofilm height dynamics and geometric constraints. (A) Biofilm height versus time is shown for a 48-hour period in linear and log scales (inset). Three replicates of *A. veronii* are shown. Height increases even at early times, as seen on the log scale. (B) Change in height is plotted against biofilm height. There are two clear regimes: (I) accelerated and (II) decelerated growth, separated by a characteristic length. (C) The height of microbial colonies grown on small agar columns, thus preventing lateral diffusion of nutrients is shown. In one set of experiments, colonies on the agar columns are replaced every two days (R). In a control set of experiments, colonies are not replaced (NR) and instead are allowed to continue growing. (D) The total height of colonies grown on individual agar columns over a period of 6 days is shown. These results demonstrate that colony height does not saturate due to nutrient depletion. (E) The thickness of the actively growing layer can be approximated as a simple minimum function, and can be used to model the two different growth regimes. Nutrient dynamics are shown for O_2 for a *E. coli* colony, with a value of L=28.26 μm

bial colony growth often directly model the transport and depletion of nutrients. In fact, a prevalent hypothesis is that the environment runs out of nutrients, leading to a decrease in biofilm growth rate and eventually a final, maximum height. While this scenario is surely relevant in many natural settings, it is unclear if it applies to typical agar plate experiments, like the ones presented here.

To evaluate the role of nutrient depletion in the vertical growth of biofilms, we grew colonies for 48 hours on polycarbonate membranes with pores large enough for nutrients to pass through but too small for bacteria to pass through, on small agar columns (3.24 cm^2 in surface area and 0.5cm tall) cut from larger agar plates. These small columns limit the role of lateral diffusion of nutrients in the agar and represent a finite environment with lateral dimensions similar to the biofilm. On typical large agar plates, nutrients diffuse horizontally and vertically; on these small columns, nutrients primarily only diffuse vertically up to the colony. After 48 hours, we removed the membrane and colony. We then immediately placed a new membrane on the used column and inoculated, for a second time, in the same location (See Figure S2 for more details). We found that despite the fact that the first colony nearly reached its saturated height(80%), the second colony grew to 75% of the same height. We then repeated this process on the same plates, i.e., we inoculated at the same location for a third time. Again, we observed that biofilms readily grew, reaching an average height 45% of their previous height. These observations were robust against 12 replicates(Figure 2C). Control plates without replacement showed a total growth of 295.4 μm, while columns with replacement grew a total of 462.1 μm, an excess of 55% (Figure 2D). These experiments demonstrate that vertical growth rates can dramatically slow despite the presence of abundant nutrients in the agar. However, these experiments do not address the impact of diffusion and uptake of nutrients within the biofilm.

C. Nutrient dynamics in the biofilm

One possible explanation for the observed "switch" between the two growth rate regimes comes from accounting for the vertical structure of the microbial colony itself. Nutrients must diffuse inside the colony(57) where they are consumed by the cells. The interplay between diffusive and uptake dynamics leads to the formation of a finite-sized active growth layer. In other words, this class of models naturally leads to two growth regimes, separated by some characteristic length. This approach is a major component of state of the art 3-dimensional biofilm models(58–62), and has been observed experimentally in different settings(63, 64). Nutrients can only enter biofilms through the biofilm-air interface that supplies oxygen to the colony, and the biofilm-substrate interface, which supplies water, carbon sources, and other macroscopic nutrients(63, 65). To determine if uptake and diffusion within a colony produces a "switch" similar to what we observe, we seek to quantify their impact on growth as a function of height above the agar-biofilm interface. The nutrient profile of the limiting nutrient $c(z,t)$, inside a 1-dimensional vertical (z) colony can be described as:

$$\frac{\partial c}{\partial t} = D \cdot \frac{\partial^2 c}{\partial z^2} - \lambda \cdot \frac{c}{k+c} \quad \textbf{(1)}$$

where D is the diffusion constant for the nutrient, λ is the consumption rate of the nutrient due to a homogeneous population, and k is the characteristic concentration in Monod kinematics. Since the limiting nutrient will be supplied through one of the colony interfaces, we set $c(0,t)$ to a constant and $\dot{c}(h,t) = 0$, where h is the height of the colony at time t. There is no analytical solution to this equation in steady state, so we solved it numerically (see Materials and Methods). This expression also captures the total growth due to Monod kinematics, $c/(k+c)$, at different distances from the interface, z, which results in the formation of a thin active region of length L (Figure 2E). The total growth N that a colony of height h will be limited by this length L, increasing when $h < L$ and then saturating in the $h \geq L$ regime. To obtain an expression for N, we first must solve Equation 1, giving us an expression that is a function of the diffusion coefficient D, consumption rate λ, and Monod constant k. As an approximation for this total growth we introduce a minimum function, that captures this saturating behavior:

$$N(h,D,\lambda,k) = \int_0^h \frac{c(z)}{k+c(z)} dz \approx \min(h,L) \quad \textbf{(2)}$$

This approximation provides a less nuanced description of the nutrient dynamics in the biofilm colony, while retaining quantitative accuracy (Figure 2E) and reducing the required number of parameters from three (D, λ, k) to a single heuristic value L.

D. Heuristic model of biofilm growth

We now assemble a heuristic model of vertical growth that takes these empirical and biophysical phenomena into account. We treat the colony as a material whose height, $h(t)$, increases over time. The vertical growth rate initially increases with increased $h(t)$, until $h(t)$ reaches the maximum active layer thickness. At this point, the vertical growth rate slowly decreases with further increases in $h(t)$. These phenomena can be captured with a simple 3-parameter differential equation:

$$\frac{dh}{dt} = \alpha \cdot \min(h,L) - \beta h \quad \textbf{(3)}$$

Where α is the growth rate, β is the decay rate, and L is the thickness of the active growing layer. This model is, in practice, a re-implementation of a simple population dynamics model pioneered by Lotka and Volterra (66, 67). Colony height (the population) grows at a fixed rate α, which is limited by nutrient consumption (through the interfacial dynamics described above Equation 2, which produce L), and decays at a rate β. This model can be rewritten as a piecewise function in relation to the critical height L:

$$\frac{dh}{dt} = \begin{cases} (\alpha-\beta)\cdot h & x \leq L \\ \alpha \cdot L - \beta \cdot h & x \geq L \end{cases} \quad \textbf{(4)}$$

By coupling a saturating growth rate from active-layer dynamics and a constantly increasing decay rate, the model captures the two-regime behavior observed experimentally and connects to core biophysical processes. It is worth noting that the growth and decay rates have slightly different interpretations than in a discrete population model:

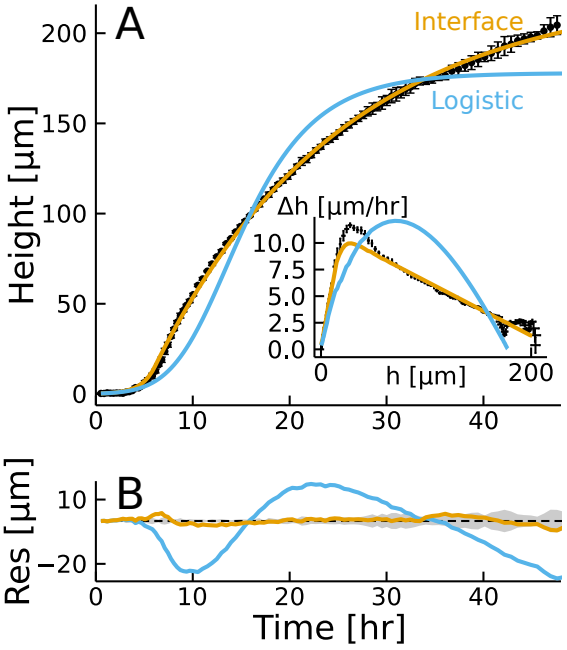

Figure 3. Quantitative assessment of the interface model for biofilm vertical growth. (A) The mean height of *A. veronii* colonies, averaged over three replicates, is shown versus time. Error bars represent standard deviation across replicates. Best fit lines for the interface and logistic models are shown. In the inset, the differential form of the models are contrasted against experimental data, showing that the interface model captures the two linear regimes in growth. (B) Residuals for the best fit predictions from the above models are shown as a function of time. On average, the logistic model by 10.77μm, and the interface model by 1.24μm. The gray region corresponds to the standard deviation of the 3 replicates in relation to the mean value at each time.

α is the height growth rate, which accounts for both cell doubling and extracellular matrix production, and β is the height decay rate, which accounts for all sources of decay, such as the incomplete reabsorption of extracellular components(68, 69), and changes in cell physiology(70).

E. Model accuracy

Over 48 hours of growth at room temperature, the interface model accurately captures colony height across the full time period (Figure 3A). The root-mean-squared error, RMSE, quantifies the relative agreement of the model: 0.15 μm, a deviation that is less than 1 cell length over two days of continuous growth. This good agreement can also be quantified with the residual as a function of time. The interface-limited model oscillates around 0 μm, with fluctuations similar to the expected differences across the 3 parallel replicates (Figure 3B).

We also compare to a logistic growth model with a coupled nutrient field that does not account for the 3-dimensional structure of the biofilm (See Materials and Methods). This model is a poor fit, with a RMSE of 10.77 μm. The logistic growth model grows slower than the experimental data at early times, and saturates at a height well below the empirical observations. A simple model of nutrient depletion in the media, absent diffusion and uptake within the colony, also fails to describe the dynamics (see Figure S5).

Finally, we investigate agreement in the change in height as a function of the current height (Figure 3A inset). The interface limited model directly incorporates the empirical relationship between Δh and h, accurately capturing the two linear regimes across development. Conversely, the lo-

gistic model completely fails to capture the observed linear relationships between growth rate and height.

F. Behavior on long time scales

We next test the agreement of the interface model on long time scales, measuring h over a period of two weeks. To do so, we measure the growth of three different species representing a wide range of microbial growth dynamics: (i) the previously introduced *A. veronii*, (ii) *E. coli*, and (iii) an aerotolerant anaerobic *S. cerevisiae* mutant. To test long term accuracy, we inoculate multiple colonies on multiple plates, and then measure all colonies on a new plate every two days (see Supplementary Information). The interface model accurately captures the vertical growth dynamics of all three microbes on long time scales (Figure 4A); all species exhibit a linear decrease in vertical growth rate, consistent with the interface model. However, the three species reach different maximum heights and do so on different time scales. For example, *A.veronii* have already reached their steady state height after 48 hours, while *S. cerevisiae* are still slowly growing after 14 days.

It is important to note that the long time agreement of the interface model does not come at the cost of accuracy on short time scales (Figure 4B). We compared the experimental data and the model predictions in the 48-hour period; for all three colonies R^2 was above 0.99. The ability to capture short and long term dynamics highlights that, in fact, vertical growth is accurately described by the simple interface model. The predicted steady state height of each biofilm can easily be obtained from the model parameters:

$$h_{\max} = \frac{\alpha \cdot L}{\beta} \qquad \textbf{(5)}$$

This expression can be used to predict the maximum height each strain reaches; experimentally measured steady state heights all fall within the 95% confidence interval for the 48 hour period. The range of this interval varies substantially across these three species (21.6 µm, 215.4 µm, and 473.23 µm for *A. veronii*, *E. coli*, and aerotolerant anaerobic *S. cerevisiae*, respectively). This wide range is rooted in the difficulty of accurately estimating β when rapid growth is still occurring (See Figure S6).

G. Universality of the vertical growth dynamics of the interface growth model

Finally, while we have thus far focused on a small number of species, the interface growth model is built on biophysical concepts that should readily apply to many species and strains. To test how broadly this model applies, we perform measurements on nine different organisms including (1) different cell sizes (from ∼1 - 10 µm), shapes (from rods to commas to nearly spherical ellipsoids), (3) different extracellular matrix production (from engineered strains with limited extracellular matrix production to wild type *V. cholerae* that are known biofilm formers), (4) prokaryotic and eukaryotic species, (5) gram positive and gram negative species, and (6) aerobic and anaerobic fungi (Table S1). We measure the vertical growth of these microbes, with three parallel replicates, for a period of 48 hours. This length of time is sufficient to capture the two growth regimes delimited by L, and thus fit all interface model parameters. We observe excellent agreement between the interface model and the vertical growth dynamics of all investigated species and strains (see Figure 5), despite differences in colony morphologies and growth rates during these 48 hours of measurement.

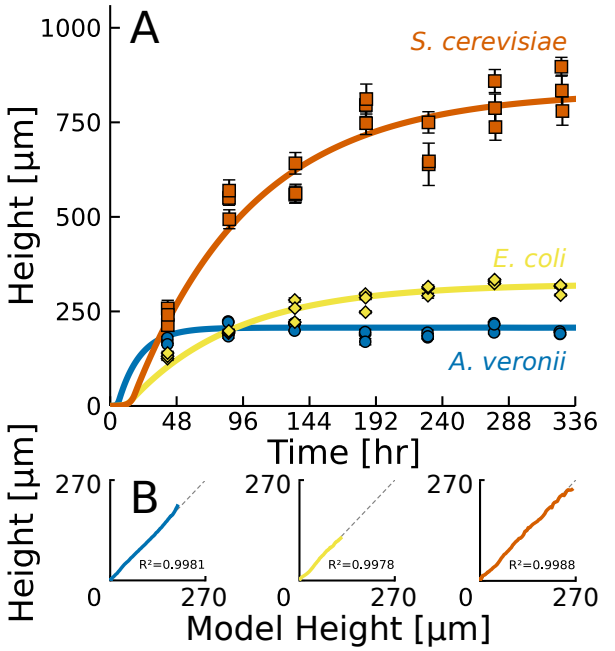

Figure 4. (A) Long-time measurements of height versus time are shown for three different species. Error bars represent standard deviations across the 2mm homeland region. Solid lines show the best-fit interface model. (B) Colony heights during the initial 48 hours of growth of plotted against best fit predictions from data taken during the 2-14 day range. The agreement between the data and the model is evident.

We summarize the allowed ranges for growth parameters in Table 1. The parameter range across the sampled cohort is quite large. α varies by a factor of ~ 4, between 0.3 hr^{-1} (*E. coli*) to 1.3 hr^{-1} (*K. pneumoniae*). L varies by a factor of ~ 6, from 7 µm (both *V. cholerae* strains) to 44 µm (*S. cerevisiae)* grown on YPD media). β is more difficult to characterize. The best fit values of β vary by a factor of ~ 4, going from 0.02 hr^{-1} to 0.09 hr^{-1} for *E. coli* and *B. cereus*, respectively. However, the confidence intervals, relative to the best fit parameter value, are typically larger for β than for α and L. Due to their large sizes, the true β values may either be nearly all ∼0.04 hr^{-1}, or distributed across a range from 0.01 hr^{-1} to 0.09 hr^{-1}.

Discussion

We investigated the vertical growth dynamics of microbial colonies using timelapse interferometry. This technique allows continuous non-disruptive measurements across broad time and length scales with single nanometer resolution, enabling us to characterize the vertical growth dynamics of microbial colonies with unprecedented precision. Using these high precision data, we found that the vertical growth rate initially increases linearly with height; after reaching a characteristic thickness, the growth rate then decreases linearly with height. We show that a simple heuristic model accurately captures short and long term dynamics. This minimal model was validated across many different species and strains of bacteria and fungi.

The dynamics of vertical growth represent a fundamen-

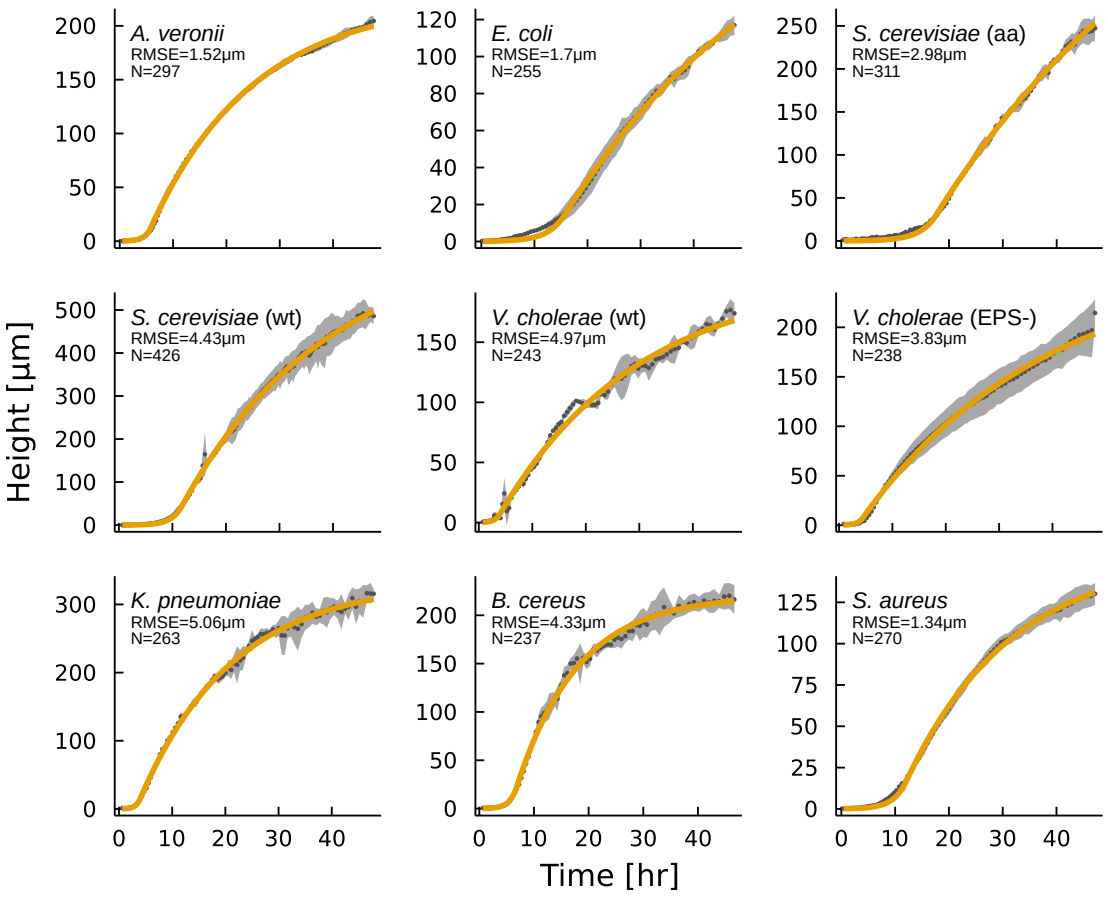

Figure 5. Growth of different species and strains over 48 hours. The average height plus or minus the standard deviation across 3 parallel colonies is shown in gray. Error bars represent standard deviation across replicates. The best fit interface model is shown in orange. The model RMSE and the total number of interferometry profiles analyzed are reported in each panel. While these microbial colonies differ in their composition, height, radius, and overall morphologies, the interface model accurately describes the average height dynamics over time for each one.

tal aspect of microbial physiology. Biofilms are exceedingly common; they are found in many environments (71–73) and are of key importance from a medical(74–78) and economic(79) perspective. An understanding of how biofilms develop their 3-dimensional structure is thus relevant for diverse questions of microbial ecology, evolution, and human health. In particular, understanding vertical growth dynamics is crucial for assessing the underlying biophysical process regarding biofilm development: the way resources do and do not limit growth, the relative fitness of various biofilm morphologies (e.g., thin biofilms vs. thick biofilms). The vertical growth measurements and model describing them are but one of the many aspects in biofilm development, but necessary ones for proper understanding how these microbial colonies grow.

The use of interferometry greatly contributed to the clarity of the empirical characterization of vertical growth dynamics presented here. For example, high resolution measurements made it abundantly clear that growth rate decreases linearly with h for $h > L$, rather than quadratically with h, despite the small size of this decay rate ($\sim$tens of nanometers per hour). These measurements were simple to perform with interferometry, which readily provides the high out-of-plane resolution necessary to capture small changes in height, is capable of performing rapid measurements to characterize changes over time, and is non-invasive so it does not disturb the colony dynamics and structure.

Interferometry, however, has three key limitations. First, this technique only measures the top surface of a colony, and cannot measure the internal structure. Second, the steepest measureable slope is limited by the numerical aperture of the objective used. When the surface is too steep ($\theta > 28.13^\circ$ for the 50x objective we used) the light path does not return to the objective. This slope threshold may limit the use of interferometry on colonies that are highly wrinkled or buckled(80–82). Finally, optical interferometry requires that a surface be sufficiently reflective. This condition will always be met for the colony-air interface; however, measurements at biofilm-fluid interfaces, while possible, are much more difficult. Despite these limitations, interferometry measurements work in a broad range of surface attached colonies and allow different models of vertical growth dynamic to be tested.

Models of biofilm growth are diverse; they incorporate different biophysical phenomena and use different mathematical approaches. However, the lack of high resolution empirical data characterizing vertical growth dynamics limited how well these models and their underlying assumptions could be tested. Crucially, the empirical data presented here have the resolution necessary to test the accuracy of existing models, evaluate their underlying assumptions, and then use empirical data to develop an accurate

Strain	$\alpha[1/hr]$	$\beta[1/hr]$	$L[\mu m]$
Aeromonas veronii	$0.878(0.853-0.942)$	$0.052(0.046-0.057)$	$13.167(11.528-14.170)$
Escherichia coli	$0.339(0.320-0.375)$	$0.023(0.006-0.047)$	$14.347(10.142-20.154)$
Saccharomyces cerevisiae (aa)	$0.345(0.334-0.354)$	$0.020(0.006-0.032)$	$30.770(25.409-34.893)$
Saccharomyces cerevisiae (wt)	$0.555(0.517-0.605)$	$0.037(0.020-0.061)$	$44.018(32.969-59.085)$
Vibrio cholerae (wt)	$1.113(0.937-1.618)$	$0.038(0.026-0.054)$	$7.066(4.126-10.223)$
Vibrio cholerae (EPS-)	$0.996(0.856-1.689)$	$0.029(0.012-0.057)$	$7.783(3.641-12.132)$
Klebsiella pneumoniae	$1.317(1.227-1.612)$	$0.057(0.046-0.068)$	$14.475(10.524-17.338)$
Bacillus cereus	$0.881(0.849-0.983)$	$0.089(0.071-0.110)$	$22.273(17.468-26.167)$
Staphylococcus aureus	$0.476(0.456-0.495)$	$0.051(0.037-0.069)$	$16.488(13.777-20.305)$

Table 1. Interface model parameters for the cohort of microbes. Shown is the best-fit, and 90% confidence interval for the 48 hour data.

heuristic model.

For example, we find that models built on logistic growth fail to capture the correct relationship between growth rate and colony height. A logistic term is functionally equivalent to a term that decreases growth rate quadratically with height. This term is mathematically appealing; it is the lowest order term that qualitatively describes the changes in growth. Despite its conceptual appeal, it lacks empirical justification (Figure 3A). Of course, most of the models developed in the literature are complex, and include more terms and fields in the set of governing equations. However, the evidence presented here suggests that going forward, logistic-like vertical growth should be replaced with empirically-supported expressions.

State of the art models of vertical growth typically include nutrient dynamics, inside and outside the biofilm. We show that, in rich media laboratory experiments, nutrient depletion in the media is not responsible for the cessation of vertical growth (Figure 2C-D). Further, we also show that accounting for the interplay between nutrient consumption and passive diffusion inside the colony is essential to accurately capture vertical growth dynamics. Thus, while nutrient dynamics in the media may need to be accounted for in some scenarios, such as growth in near starvation conditions, nutrient dynamics within the colony must always be accounted for.

Our empirical measurements demonstrate that at least three parameters are necessary to fully describe vertical growth dynamics. To this end, we proposed a heuristic "interface model" motivated by three fundamental biophysical quantities. L is the length at which growth rate ceases to increase in proportion to biofilm height. This term is inspired by, and consistent with, the length at which diffusion and uptake limit the transportation of nutrients within the biofilm. The growth rate α captures all vertical growth, including the growth and doubling of cells, but also secretion of extracellular substances. The decay rate β captures all effects that decrease growth rate, such as mechanical settling, cell death and lysis, cells entering a lag phase, and diminished efficiency in the reabsorption of biomass. In other words, α and β coarse grain all phenomena that lead to an increase or decrease (respectively) in growth rate into two simple terms. Rather than limiting the utility of this model, coarse graining places the emphasis on the net impact of increased height on growth rates, which may be universal, rather than on the microscopic mechanisms that modify growth rates, which will often be specific and heterogeneous. This approach provides a useful heuristic model for vertical growth dynamics, as opposed to more complex alternatives(50). In the following paragraphs, we compare our measurements of Ł and α against independent measurements in the literature. To our knowledge, β has not previously been measured, so such a comparison is not possible.

We now compare the values of the growth layer L that we measure to those from the literature. In *E. coli*, reports range between 3-20 µm for the zone of active growth (e.g.,(27, 62)). For *E. coli* growing on LB agar, the limiting nutrient is known to be the aminoacid L-serine(83). With this knowledge, and the necessary empirically measured parameters, we can calculate the expected thickness of the active growing layer, i.e., L, for our experimental conditions using Equation 1. Such a calculation produces a diffusion length of L=14.80µm, consistent with our measured best fit value of L=14.35µm. In *S. cerevisiae*, results using an effective medium theory and confocal measurements report L = 50 µm (84), comparable to our measurements in the wild-type strain of L = 44.02 µm.

As for growth rate, our measurement includes all contributions to vertical growth, which includes cellular reproduction but also EPS and empty space between cells. Further, comparisons are tricky as experimental details vary (e.g., strain used, temperature of incubation, inoculant volume, all of which can impact growth rate). However, for wild type *S. cerevisiae*, anaerobic *S. cerevisiae*, and *E. coli*, our measurements of α are within a factor of 2 of values measured in the literature. Specifically, $0.56hr^{-1}$, $0.35hr^{-1}$, and $0.34hr^{-1}$, and previous experiments report $0.2-0.35hr^{-1}$ [cite], $0.25hr^{-1}$(85), and $0.6hr^{-1}$(86), for *S. cerevisiae*, anaerobic *S. cerevisiae*, and *E. coli*, respectively. Thus, the α values we measure are all within a factor of ~ 2 of the values from the literature. Though imperfect, this comparison suggests that the growth rates we measure are reasonably within a physiologically relevant regime.

As the interface model is a simple heuristic model for vertical growth, there are many details it does not address. For example, the model predicts the dynamics of the bulk height, and does not distinguish between cells and extracellular matrix within the colony. Relatedly, the model focuses on the mean height and does not address spatial fluctuations. Topographic fluctuations likely encode insight into the underlying phenomena behind vertical growth dynamics, as previously demonstrated in homeostatic biofilms and tissues (87–89). In a different vein, the model does not account for more complex environmental conditions, such as limited access to nutrients(90), environmental stresses(91), or heterogeneities in the surface on which the colony grows(92). Further, in nature

biofilms often contain multiple interacting species and subpopulations(93), leading to complex dynamics (5, 94) that we do not consider here. Nonetheless, the results presented here provide a foundation on which detailed questions about vertical growth dynamics can be studied.

To that end, the diverse array of strains we measured allow for useful comparisons. First, we investigate the role of respiration in *S. cerevisiae* on vertical growth dynamics. The aerobic yeast strain used in this study is "mixotrophic," capable of both fermentation and aerobic respiration(95) depending on the concentration and types of sugars found in the environment. The anaerobic strain has lost part of its mitochondrial genome and is therefore only capable of fermentation, which is not oxygen-dependent (96). Despite these differences in cell biology, we find that there is no qualitative difference between the vertical growth dynamics of aerobic and obligate anaerobic strains of *S. cerevisiae*; the aerobic strain has larger α and L than the anaerobic strain, but in each case vertical growth dynamics proceed following the interface model. While a previous study suggests that oxygen is the limiting nutrient for the mixotrophic strain (96), further work is necessary to prove it definitively. Nonetheless, these results suggest that vertical growth is qualitatively similar regardless of if the limiting nutrient enters from the top or bottom interface.

In a different vein, we investigate the role of extracellular matrix production in *Vibrio cholerae*. We directly compare the vertical growth dynamics of strains of *V. cholerae* with and without EPS. Vibrio polysaccharide is an essential component for biofilm formation, and the associated genes are controlled by the master biofilm regulator, VpsR(97, 98). Deletion of *vpsR* (EPS- mutant) prevents biofilm production in *V. cholerae*, leading instead to the growth of colonies with a smooth morphology that produce less EPS than their wildtype counterparts(97). Comparing these stains allows us to compare the impact of the amount of potentially "active" biomass (cells), and inactive biomass (EPS). We find that both strains are well-fit by the interface model. Further, the vertical growth dynamics are quantitatively very similar, regardless of the presence or absence of EPS. Thus, this comparison suggests that microbial colony vertical growth dynamics proceed similarly, even as extracellular matrix production varies.

The results presented here suggest that a linear decay of vertical growth rate may be a fundamental aspect of biofilm physiology. However, future work will be necessary to understand the mechanistic origins of this decay, as well as how to quantitatively connect such mechanisms to measurements of β. To that end, there are many physiological differences between cells in and out of the active growing layer, as well as across the colony (70, 99). The "inactive" cells may change their metabolism, enter the stationary phase, change their EPS production, or sporulate, among many other possibilities. While a decrease in nutrient concentration in the media may also slow growth rates, many microbes exhibit a complex relationship between growth rate and nutrient concentration; this function need not even be monotonic(100). Nonetheless, the decrease in growth rate due to a colony-wide decay means that colony can cease even when there are plenty of nutrients in the environment. Thus, while future studies are necessary to rigorously link β to its specific causes, this linear decay represents a biophysical constraint that limits biofilm growth.

The study of microbial community interfaces via interferometry presents an easy and inexpensive approach to studying the structure of microbial colonies. Interfaces and surface fluctuations have long been studied in physics, both for the information they provide about what occurs beneath the surface as well as the rich phenomena that surfaces themselves exhibit. Indeed, biology also has a rich history of studying interfaces, from the surfaces of cells or organs(101–104), to biome-scale interfaces(105). Biological interfaces on meso-scales are traditionally less studied, despite their known importance in a wide range of systems(106–108) including bacterial communities (58, 109). This is likely due to the difficulty in measuring these microscopic, and often sticky, interfaces. Other techniques for characterizing the height and topographies of colonies lack the resolution (e.g., confocal microscopy), are slow and potentially destructive (e.g., atomic force microscopy), or do not readily permit time lapse measurements (e.g., scanning electron microscopy)(39). While these alternative measurement techniques might be modified to overcome their limitations(110), interferometry is already very well-suited for studying biofilm topographies, as demonstrated here and in previous studies (32, 88, 89). These works represent the first attempts to utilize optical interferometry as a tool for microbiology, an approach that will only grow more useful when paired with the development of heuristic models and detailed measurement protocols.

Materials and Methods

Interferometry Timelapses

All inoculations consist of 1.5 µL from an overnight culture grown at 37 °C diluted to OD_{600}=1. Control plates were left to grow at a temperature of 23.8 °C. Since colony growth is radially symmetric, we only measure a horizontal strip of the biofilm, allowing us to achieve better temporal resolution. The measurement proceeds across the entire colony, and includes uncolonized substrate surface on both sides of the colony. Given the aspect ratio of our data and the goals of our study, we then lower the dimension of the data by averaging on the Y-axis (Figure 1A-C). Then, we utilize the substrate height measurements to obtain the relative height of the colony to its background.

Column growth

We label and cut columns of LB agar to dimensions of 18mm$\times$18mm$\times$5mm. On each column we deposited a Polycarbonate Track Etch Membrane with 0.2 µm pore size, 13mm diameter (GVS brand). We inoculate 1.5µL of OD1 bacterial suspension on top of said membrane. This is repeated over 6 plates (18 columns/colonies). Every 48 hours, up to 3 iterations, we measure the growth on each column. On 9 of the columns we than removed the membrane and immediately deposited a new membrane and inoculated on top of the new membrane.

Nutrient concentrations inside the colony

The nutrient profile of the limiting nutrient $c(z)$, assuming that growth of the biofilm colony is a slow process, we can write the dynamics for the nutrient inside a 1-dimensional colony as:

$$\frac{\partial c}{\partial t} = D \cdot \frac{\partial^2 c}{\partial z^2} - \lambda \cdot \frac{c}{k+c} \quad \textbf{(6)}$$

We set the boundary conditions $c(0,t) = c_0$, and $\dot{c}(L,t) = 0$ to simulate the dynamics in a closed colony with the nutrients only entering through one side.

This problem has no simple analytical solution, but can be numerically integrated until it reaches a steady state. For the main text example we utilize $D = 2500\mu m^2 \cdot s^{-1}$, $c_0 = 250\mu M$, $\lambda = 1.6 \cdot 10^3 \mu M \cdot s^{-1}$, $k = 1\mu M$, values corresponding to the diffusion of Oxygen diffusing through a dense *E. coli* colony (62, 111, 112). These parameters lead to a limit length $L = 28.264\mu m$, which is obtained empirically by the best-fit minimum function to the cumulative value of the monod growth term.

Utilizing values corresponding for nutrient-limitation from the substrate, such as L-serine in LB agar($D = 800\mu m^2 \cdot s^{-1}$, $c_0 = 100\mu M$, $\lambda = 1.3 \cdot 10^3 \mu M \cdot s^{-1}$, $k = 38\mu M$)(83). The value obtained is $L = 14.801\mu m$.

Growth models and ODE simulations

Interface model. The interface model, is the 3-parameter heuristic model introduced in the main text. The model is governed by one simple equation for the colony height h:

$$\frac{dh}{dt} = \alpha \cdot \min(h, L) - \beta \cdot h \quad \textbf{(7)}$$

Where α is the growth rate, β the decay rate, and L the width of the growing region in the colony.

Logistic model. As an alternative for quick-comparisons between the models we implement the colony h utilizing logistic growth, and consuming a nutrient supply c in a non-spatial manner:

$$\frac{dh}{dt} = \alpha \cdot h \cdot \frac{c}{K_c + c} \cdot \left(1 - \frac{h}{K}\right) \quad \textbf{(8)}$$

$$\frac{dc}{dt} = -\epsilon \cdot \alpha \cdot h \cdot \frac{c}{K_c + c} \quad \textbf{(9)}$$

Where α is the colony growth rate, K the carrying capacity, K_c the Monod constand for nutrient uptake, ϵ the inverse conversion from nutrients to biofilm biomass.

Data availability

Source code for the cleaning, analysis and figures, and clean datasets have been uploaded to a Github repository. Due to file size limits, full unprocessed images are available upon request.

Acknowledgments

P.J.Y. acknowledges funding from the NIH NIGMS (Grant No. 1R35GM138354-01) and NSF Biomaterials (Grant No. BMAT2003721). B.K.H. acknowledges funding from NSF Biomaterials (Grant No. BMAT2003721).

Bibliography

1. P Watnick, R Kolter, Biofilm, city of microbes. *Journal of Bacteriology* **182**, 2675–2679 (2000) Publisher: Am Soc Microbiol.
2. HC Flemming, et al., Biofilms: an emergent form of bacterial life. *Nature Reviews Microbiology* **14**, 563–575 (2016).
3. L Hall-Stoodley, JW Costerton, P Stoodley, Bacterial biofilms: from the natural environment to infectious diseases. *Nature Reviews Microbiology* **2**, 95–108 (2004).
4. G Lambert, A Bergman, Q Zhang, D Bortz, R Austin, Physics of biofilms: The initial stages of biofilm formation and dynamics. *New Journal of Physics* **16** (2014) Publisher: IOP Publishing.
5. CD Nadell, K Drescher, KR Foster, Spatial structure, cooperation and competition in biofilms. *Nature Reviews Microbiology* **14**, 589–600 (2016).
6. J Wille, T Coenye, Biofilm dispersion: The key to biofilm eradication or opening Pandora's box? *Biofilm* **2**, 100027 (2020).
7. B D'Acunto, L Frunzo, I Klapper, M Mattei, Modeling multispecies biofilms including new bacterial species invasion. *Mathematical biosciences* **259**, 20–26 (2015).
8. P Ghosh, H Levine, Morphodynamics of a growing microbial colony driven by cell death. *Physical Review E* **96**, 1–8 (2017).
9. X Wang, HA Stone, R Golestanian, Shape of the growing front of biofilms. *New Journal of Physics* **19**, 125007 (2017) Publisher: IOP Publishing.
10. DvHt Echten, G Nordemann, M Wehrens, S Tans, T Idema, Defect dynamics in growing bacterial colonies. *arXiv preprint arXiv: 2003.10509* pp. 1–17 (2020) arXiv: 2003.10509.
11. C Fei, et al., Nonuniform growth and surface friction determine bacterial biofilm morphology on soft substrates. *Proceedings of the National Academy of Sciences* **117**, 7622–7632 (2020) Publisher: Proceedings of the National Academy of Sciences.
12. L Xiong, et al., Flower-like patterns in multi-species bacterial colonies. *Elife* **9**, e48885 (2020).
13. GT Fortune, NM Oliveira, RE Goldstein, Biofilm Growth under Elastic Confinement. *Physical Review Letters* **128**, 178102 (2022) Publisher: American Physical Society.
14. AKY Tam, B Harding, JEF Green, S Balasuriya, BJ Binder, Thin-film lubrication model for biofilm expansion under strong adhesion. *Physical Review E* **105**, 014408 (2022) Publisher: American Physical Society.
15. JA Moore-Ott, S Chiu, DB Amchin, T Bhattacharjee, SS Datta, A biophysical threshold for biofilm formation. *eLife* **11**, e76380 (2022).
16. D De Beer, P Stoodley, F Roe, Z Lewandowski, Effects of biofilm structures on oxygen distribution and mass transport. *Biotechnology and bioengineering* **43**, 1131–1138 (1994).
17. PS Stewart, et al., Reaction–diffusion theory explains hypoxia and heterogeneous growth within microbial biofilms associated with chronic infections. *NPJ biofilms and microbiomes* **2**, 1–8 (2016).
18. J Yan, AG Sharo, HA Stone, NS Wingreen, BL Bassler, Vibrio cholerae biofilm growth program and architecture revealed by single-cell live imaging. *Proceedings of the National Academy of Sciences* **113**, E5337–E5343 (2016).
19. F Beroz, et al., Verticalization of bacterial biofilms. *Nature Physics* **14**, 954–960 (2018) Number: 9 Publisher: Nature Publishing Group.
20. NM Oliveira, et al., Biofilm formation as a response to ecological competition. *PLoS biology* **13**, e1002191 (2015).
21. O Rendueles, JM Ghigo, Mechanisms of competition in biofilm communities. *Microbial Biofilms* pp. 319–342 (2015).
22. KZ Coyte, H Tabuteau, EA Gaffney, KR Foster, WM Durham, Microbial competition in porous environments can select against rapid biofilm growth. *Proceedings of the National Academy of Sciences* **114**, E161–E170 (2017).
23. G Steinbach, C Crisan, SL Ng, BK Hammer, PJ Yunker, Accumulation of dead cells from contact killing facilitates coexistence in bacterial biofilms. *Journal of the Royal Society Interface* **17**, 20200486 (2020).
24. J Monod, The growth of bacterial cultures. *Selected Papers in Molecular Biology by Jacques Monod* **139** (2012).
25. RJ Allen, B Waclaw, Bacterial growth: a statistical physicist's guide. *Reports on Progress in Physics* **82**, 016601 (2019) 00000.
26. A Cooper, A Dean, CN Hinshelwood, Factors affecting the growth of bacterial colonies on agar plates. *Proceedings of the Royal Society of London. Series B. Biological Sciences* **171**, 175–199 (1968).
27. MR Warren, et al., Spatiotemporal establishment of dense bacterial colonies growing on hard agar. *eLife* **8**, 1–47 (2019).
28. M Basaran, YI Yaman, TC Yüce, R Vetter, A Kocabas, Large-scale orientational order in bacterial colonies during inward growth. *Elife* **11**, e72187 (2022).
29. ME Davey, GA O'toole, Microbial biofilms: from ecology to molecular genetics. *Microbiology and molecular biology reviews* **64**, 847–867 (2000).
30. RM Donlan, Biofilm formation: a clinically relevant microbiological process. *Clinical infectious diseases* **33**, 1387–1392 (2001).
31. J Dervaux, JC Magniez, A Libchaber, On growth and form of Bacillus subtilis biofilms. *Interface Focus* **4** (2014).
32. C Larimer, JD Suter, G Bonheyo, RS Addleman, In situ non-destructive measurement of biofilm thickness and topology in an interferometric optical microscope. *Journal of Biophotonics* **9**, 656–666 (2016) _eprint: https://onlinelibrary.wiley.com/doi/pdf/10.1002/jbio.201500212.
33. S Kesel, et al., Matrix composition determines the dimensions of Bacillus subtilis NCIB 3610 biofilm colonies grown on LB agar. *RSC Advances* **7**, 31886–31898 (2017) Publisher: The Royal Society of Chemistry.
34. M Werb, et al., Surface topology affects wetting behavior of Bacillus subtilis biofilms. *npj Biofilms and Microbiomes* **3**, 1–10 (2017) Number: 1 Publisher: Nature Publishing Group.
35. J Schiebel, et al., Analysis of three-dimensional biofilms on different material surfaces. *Biomaterials Science* **8**, 3500–3510 (2020) Publisher: Royal Society of Chemistry.
36. AJ Paula, G Hwang, H Koo, Dynamics of bacterial population growth in biofilms resemble spatial and structural aspects of urbanization. *Nature Communications* **11**, 1354 (2020) Number: 1 Publisher: Nature Publishing Group.
37. EN Hayta, CA Rickert, O Lieleg, Topography quantifications allow for identifying the contribution of parental strains to physical properties of co-cultured biofilms. *Biofilm* **3**, 100044 (2021).
38. KU Mahto, S Das, Microscopic techniques to evaluate the biofilm formation ability of a marine bacterium Pseudomonas aeruginosa PFL-P1 on different substrata. *Microscopy Research and Technique* **84**, 2451–2461 (2021) _eprint:

https://onlinelibrary.wiley.com/doi/pdf/10.1002/jemt.23799.
39. Y Huang, S Chakraborty, H Liang, Methods to probe the formation of biofilms: applications in foods and related surfaces. *Analytical Methods* **12**, 416–432 (2020) Publisher: The Royal Society of Chemistry.
40. MG Mazza, The physics of biofilms - An introduction. *Journal of Physics D: Applied Physics* **49** (2016) arXiv: 1606.01392 Publisher: IOP Publishing.
41. MR Mattei, et al., Continuum and discrete approach in modeling biofilm development and structure: a review. *Journal of Mathematical Biology* **76**, 945–1003 (2018) MAG ID: 2739410635.
42. H Nguyen, Y A, Abraham Ybarra, H Başağaoğlu, O Shindell, Biofilm viscoelasticity and nutrient source location control biofilm growth rate, migration rate, and morphology in shear flow. *Scientific Reports* **11**, 16118 (2021) MAG ID: 3188109131.
43. E Alpkvist, C Picioreanu, MCM van Loosdrecht, A Heyden, Three-dimensional biofilm model with individual cells and continuum EPS matrix. *Biotechnology and Bioengineering* **94**, 961–979 (2006) Publisher: Wiley Online Library.
44. T Zhang, NG Cogan, Q Wang, Phase-Field models for biofilm. I. Theory and 1-D simulations. *Siam Journal On Applied Mathematics* **69**, 641–669 (2008).
45. R Hartmann, et al., Emergence of three-dimensional order and structure in growing biofilms. *Nature Physics* **15**, 251–256 (2019) Publisher: Springer US.
46. S Srinivasan, CN Kaplan, L Mahadevan, A multiphase theory for spreading microbial swarms and films. *eLife* **8**, 8–10 (2019).
47. X Jin, JS Marshall, MJ Wargo, Hybrid Model of Bacterial Biofilm Growth. *Bulletin of Mathematical Biology* **82**, 27–27 (2020) MAG ID: 3003693092.
48. A Tam, et al., A thin-film extensional flow model for biofilm expansion by sliding motility. *Proceedings of the Royal Society A: Mathematical, Physical and Engineering Sciences* **475**, 20190175 (2019) Publisher: Royal Society.
49. J Hughes, A Mathematical Model of Biofilm Growth on Degradable Substratum. *SIAM Undergraduate Research Online* **13** (2020).
50. R Levins, The strategy of model building in population biology. *American scientist* **54**, 421–431 (1966).
51. J Gunawardena, Models in biology:'accurate descriptions of our pathetic thinking'. *BMC biology* **12**, 1–11 (2014).
52. EE Bernardy, MA Turnsek, SK Wilson, CL Tarr, BK Hammer, Diversity of clinical and environmental isolates of vibrio cholerae in natural transformation and contact-dependent bacterial killing indicative of type vi secretion system activity. *Applied and environmental microbiology* **82**, 2833–2842 (2016).
53. D Yanni, et al., Life in the coffee-ring: how evaporation-driven density gradients dictate the outcome of inter-bacterial competition. *arXiv preprint arXiv:1707.03472* (2017).
54. A Agrawal, S Sinha, R Mukherjee, D Mampallil, Dynamics of bacterial deposition in evaporating drops. *Physics of Fluids* **32**, 093308 (2020).
55. RL Bertrand, Lag phase is a dynamic, organized, adaptive, and evolvable period that prepares bacteria for cell division. *Journal of bacteriology* **201**, e00697–18 (2019).
56. PG Hamill, et al., Microbial lag phase can be indicative of, or independent from, cellular stress. *Scientific reports* **10**, 1–20 (2020).
57. PS Stewart, Diffusion in Biofilms. *Journal of Bacteriology* **185**, 1485–1491 (2003) 01179.
58. JA Bonachela, CD Nadell, JB Xavier, SA Levin, Universality in bacterial colonies. *Journal of Statistical Physics* **144**, 303–315 (2011).
59. F. D. C. Farrell, F Farrell, O Hallatschek, D Marenduzzo, B Waclaw, Mechanically driven growth of quasi-two dimensional microbial colonies. *Physical Review Letters* **111**, 168101–168101 (2013) MAG ID: 1994889554.
60. G Melaugh, et al., Shaping the growth behaviour of biofilms initiated from bacterial aggregates. *PloS one* **11**, e0149683 (2016).
61. E Young, G Melaugh, RJ Allen, Pinning transition in biofilm structure driven by active layer dynamics. *bioRxiv* (2022).
62. A Martínez-Calvo, et al., Morphological instability and roughening of growing 3d bacterial colonies. *Proceedings of the National Academy of Sciences* **119**, e2208019119 (2022).
63. KD Xu, PS Stewart, F Xia, CT Huang, GA McFeters, Spatial physiological heterogeneity in pseudomonas aeruginosa biofilm is determined by oxygen availability. *Applied and environmental microbiology* **64**, 4035–4039 (1998).
64. I Klapper, JD Dockery, Mathematical Description of Microbial Biofilms. *Siam Review* **52**, 221–265 (2010) MAG ID: 2024995147.
65. PS Stewart, MJ Franklin, Physiological heterogeneity in biofilms. *Nature Reviews Microbiology* **6**, 199–210 (2008).
66. AJ Lotka, *Elements of physical biology*. (Williams & Wilkins), (1925).
67. V Volterra, Fluctuations in the abundance of a species considered mathematically. *Nature* **118**, 558–560 (1926).
68. RD Monds, GA O'Toole, The developmental model of microbial biofilms: ten years of a paradigm up for review. *Trends in microbiology* **17**, 73–87 (2009).
69. KW Bayles, Bacterial programmed cell death: making sense of a paradox. *Nature Reviews Microbiology* **12**, 63–69 (2014).
70. JS Webb, M Givskov, S Kjelleberg, Bacterial biofilms: prokaryotic adventures in multicellularity. *Current opinion in microbiology* **6**, 578–585 (2003).
71. WC Ghiorse, JT Wilson, Microbial ecology of the terrestrial subsurface. *Advances in applied microbiology* **33**, 107–172 (1988).
72. MC Horner-Devine, KM Carney, BJ Bohannan, An ecological perspective on bacterial biodiversity. *Proceedings of the Royal Society of London. Series B: Biological Sciences* **271**, 113–122 (2004).
73. F Azam, F Malfatti, Microbial structuring of marine ecosystems. *Nature Reviews Microbiology* **5**, 782–791 (2007).
74. JD Bryers, Medical biofilms. *Biotechnology and bioengineering* **100**, 1–18 (2008).
75. G Zhao, et al., Biofilms and inflammation in chronic wounds. *Advances in wound care* **2**, 389–399 (2013).
76. S Veerachamy, T Yarlagadda, G Manivasagam, PK Yarlagadda, Bacterial adherence and biofilm formation on medical implants: a review. *Proceedings of the Institution of Mechanical Engineers, Part H: Journal of Engineering in Medicine* **228**, 1083–1099 (2014).
77. YM Wi, R Patel, Understanding biofilms and novel approaches to the diagnosis, prevention, and treatment of medical device-associated infections. *Infectious Disease Clinics* **32**, 915–929 (2018).
78. D Sharma, L Misba, AU Khan, Antibiotics versus biofilm: an emerging battleground in microbial communities. *Antimicrobial Resistance & Infection Control* **8**, 1–10 (2019).
79. M Cámara, et al., Economic significance of biofilms: a multidisciplinary and cross-sectoral challenge. *npj Biofilms and Microbiomes* **8**, 1–8 (2022).
80. LE Dietrich, et al., Bacterial community morphogenesis is intimately linked to the intracellular redox state. *Journal of bacteriology* **195**, 1371–1380 (2013).
81. JN Wilking, et al., Liquid transport facilitated by channels in bacillus subtilis biofilms. *Proceedings of the National Academy of Sciences* **110**, 848–852 (2013).
82. J Yan, et al., Mechanical instability and interfacial energy drive biofilm morphogenesis. *Elife* **8**, e43920 (2019).
83. OA Croze, GP Ferguson, ME Cates, WC Poon, Migration of chemotactic bacteria in soft agar: role of gel concentration. *Biophysical journal* **101**, 525–534 (2011).
84. MO Lavrentovich, JH Koschwanez, DR Nelson, Nutrient shielding in clusters of cells. *Physical Review E* **87**, 062703 (2013).
85. M Zakhartsev, M Reuss, Cell size and morphological properties of yeast saccharomyces cerevisiae in relation to growth temperature. *FEMS yeast research* **18**, foy052 (2018).
86. A Farewell, FC Neidhardt, Effect of temperature on in vivo protein synthetic capacity in escherichia coli. *Journal of bacteriology* **180**, 4704–4710 (1998).
87. T Risler, A Peilloux, J Prost, Homeostatic fluctuations of a tissue surface. *Physical review letters* **115**, 258104 (2015).
88. A Kalziqi, et al., Immotile Active Matter: Activity from Death and Reproduction. *Physical Review Letters* **120**, 18101 (2018) Publisher: American Physical Society.
89. A Kalziqi, et al., Viscosity independent diffusion mediated by death and reproduction in biofilms. *arXiv preprint arXiv: 1901.01350* (2019) arXiv: 1901.01350.
90. MR Chénier, et al., Impact of seasonal variations and nutrient inputs on nitrogen cycling and degradation of hexadecane by replicated river biofilms. *Applied and Environmental Microbiology* **69**, 5170–5177 (2003).
91. E Tsagkari, S Connelly, Z Liu, A McBride, WT Sloan, The role of shear dynamics in biofilm formation. *npj Biofilms and Microbiomes* **8**, 1–10 (2022).
92. M Gralka, O Hallatschek, Environmental heterogeneity can tip the population genetics of range expansions. *Elife* **8**, e44359 (2019).
93. A Stacy, L McNally, SE Darch, SP Brown, M Whiteley, The biogeography of polymicrobial infection. *Nature Reviews Microbiology* **14**, 93–105 (2016).
94. M Ghoul, S Mitri, The ecology and evolution of microbial competition. *Trends in microbiology* **24**, 833–845 (2016).
95. R De Deken, The crabtree effect: a regulatory system in yeast. *Microbiology* **44**, 149–156 (1966).
96. GO Bozdag, E Libby, R Pineau, CT Reinhard, WC Ratcliff, Oxygen suppression of macroscopic multicellularity. *Nature communications* **12**, 1–10 (2021).
97. FH Yildiz, NA Dolganov, GK Schoolnik, Vpsr, a member of the response regulators of the two-component regulatory systems, is required for expression of vps biosynthesis genes and epsetr-associated phenotypes in vibrio cholerae o1 el tor. *Journal of bacteriology* **183**, 1716–1726 (2001).
98. JC Fong, KA Syed, KE Klose, FH Yildiz, Role of vibrio polysaccharide (vps) genes in vps production, biofilm formation and vibrio cholerae pathogenesis. *Microbiology* **156**, 2757 (2010).
99. JV Gestel, H Vlamakis, R Kolter, Division of labor in biofilms: the ecology of cell differentiation. *Microbial Biofilms* pp. 67–97 (2015).
100. H Youk, A Van Oudenaarden, Growth landscape formed by perception and import of glucose in yeast. *Nature* **462**, 875–879 (2009).
101. DJ Cosgrove, Growth of the plant cell wall. *Nature reviews molecular cell biology* **6**, 850–861 (2005).
102. NJ Abbott, AA Patabendige, DE Dolman, SR Yusof, DJ Begley, Structure and function of the blood–brain barrier. *Neurobiology of disease* **37**, 13–25 (2010).
103. L Shen, CR Weber, DR Raleigh, D Yu, JR Turner, Tight junction pore and leak pathways: a dynamic duo. *Annual review of physiology* **73**, 283 (2011).
104. T Harayama, H Riezman, Understanding the diversity of membrane lipid composition. *Nature reviews Molecular cell biology* **19**, 281–296 (2018).
105. L Erdős, et al., Habitat heterogeneity as a key to high conservation value in forest-grassland mosaics. *Biological Conservation* **226**, 72–80 (2018).
106. QX Liu, et al., Phase separation explains a new class of self-organized spatial patterns in ecological systems. *Proceedings of the National Academy of Sciences* **110**, 11905–11910 (2013).
107. SJ Turley, V Cremasco, JL Astarita, Immunological hallmarks of stromal cells in the tumour microenvironment. *Nature reviews immunology* **15**, 669–682 (2015).
108. B Ladoux, RM Mège, Mechanobiology of collective cell behaviours. *Nature reviews Molecular cell biology* **18**, 743–757 (2017).
109. SJ Kassinger, ML van Hoek, Biofilm architecture: An emerging synthetic biology target. *Synthetic and Systems Biotechnology* **5**, 1–10 (2020).
110. N Raab, I Bachelet, Resolving biofilm topography by native scanning electron microscopy. *Journal of Biological Methods* **4**, e70–e70 (2017) Number: 2.
111. C Douarche, A Buguin, H Salman, A Libchaber, E. coli and oxygen: a motility transition. *Physical review letters* **102**, 198101 (2009).
112. X Fu, et al., Spatial self-organization resolves conflicts between individuality and collective migration. *Nature communications* **9**, 1–12 (2018).

Vertical growth dynamics of biofilms - Supplementary Information

Pablo Bravo, Siu Lung Ng, Kathryn A. MacGillivray, Brian K. Hammer, and Peter J. Yunker

Interferometry timelapses

We grow an overnight at 37°celsius of all microbial species, then back-dilute to an optical density (OD_{600}) of 1, and inoculate in an Lysogeny Broth (LB) Agar 1.5% plate for bacterial colonies, and Yeast Extract Peptone Dextrose (YPD) Agar 1.5% for *S. cerevisiae* colonies, an amount of 1.5 µL. Measurements were performed on a Zygo ZeGage Pro optical interferometer, enclosed by a custom plastic casing that allows continuous measurements with minimal media and sample evaporation. The full enclosure maintains a temperature of 23.8 °C and a relative humidity of 80% for the full measuring period. Details for the media are reported below:

- **LB Agar**: 10g tryptone, 5g yeast extract, 10g NaCl, 15 g agar in 1 liter of water.
- **YPD Agar**: 20g dextrose, 20g peptone, 10g yeast extract, and 15g agar in 1 liter of water.

Strain	Species	Media	Details	Cell shape	Gram
ZOR0001	*Aeromonas veronii*	LB 1.5%	wild type	rod	negative
MG1655	*Escherichia coli*	LB 1.5%	wild type	rod	negative
GOB33	*Saccharomyces cervisiae*	YPD	petite yeast	ellipsoid	-
Y55	*Saccharomyces cervisiae*	YPD	wild type	ellipsoid	-
C6706	*Vibrio cholerae*	LB 1.5%	wild type	comma	negative
C6706	*Vibrio cholerae*	LB 1.5%	Δ*vpsR*	comma	negative
Top52	*Kelbsiella pneumoniae*	LB 1.5%	wild type	rod	negative
SW520	*Bacillus cereus*	LB 1.5%	wild type	rod	positive
SW519	*Staphylococcus aureus*	LB 1.5%	wild type	spherical	positive

Table S1. Timelapses overview details, for the microbial strains and growth media.

A. 48h timelapses

On two 1.5% LB agar plate, we inoculated 3 colonies of the measured strain in each. One plate was measured continuously (replicates A-C) for 48 hours in the profilometer enclosure, the other plate was left sealed with Parafilm growing at 23.8 °C for the same duration of 48 hours. Measurements consist of horizontal radial strips of each colony with a 50x Mirau objective (NA 0.55), on the 1000x200 @800Hz capture mode. We increase the Field of View of the measurement adaptively, to always capture an uncolonized region outside the growing colony. Colonies that were continuously measured did not show any significant growth differences compared to their sealed counterparts (replicates D-F) after the experiment (Figure S1).

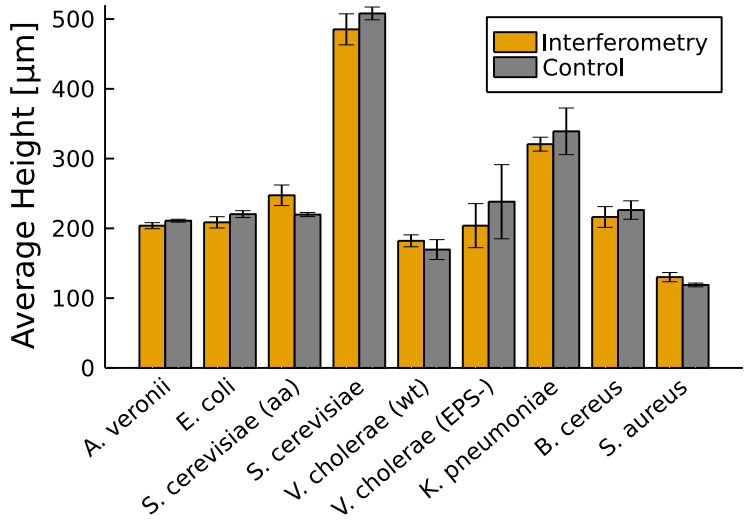

Figure S1. Colony heights are not affected by continuous measurement under the interferometer. Control samples were grown for the same amount of time without continuous measurement. Comparisons were after each timelapse finished, at 48.6, 87.7, 47.6, 48.6, 49.5, 50.2, 48.3, 47.1, 47.48 hours respectively.

B. Long time measurements

We inoculated 21 plates 7 for ZOR0001, 7 MG1655, and 7 GOB33 (Table S1), with 3 separate colonies each. All plates were sealed with parafilm after inoculation. Every two days, we performed radial measurements with a 10x Mirau objective (NA 0.3) 1000x200 @800Hz capture mode. Each plate was discarded after measurement.

Heuristic Interface Model

A. Empirical basis

To explore the role of nutrient depletion in the agar directly below the colonies, we devised an experiment that would explore the limits of how much growth is allowed in a vertical column of agar.

We label and cut columns of LB agar to dimensions of 18mm$\times$18mm$\times$5mm. On each column we deposited a Polycarbonate Track Etch Membrane with 0.2 µm pore size, 13mm diameter (GVS brand). We inoculate 1.5µL of OD_{600}=1 bacterial suspension on top of said membrane. This is repeated over 6 plates (18 columns/colonies). Every 48 hours, up to 3 iterations, we measure the growth on each column. On 9 of the columns we then removed the membrane and immediately (<5 minutes) deposited a new membrane and inoculated on top of the new membrane (Figure S2).

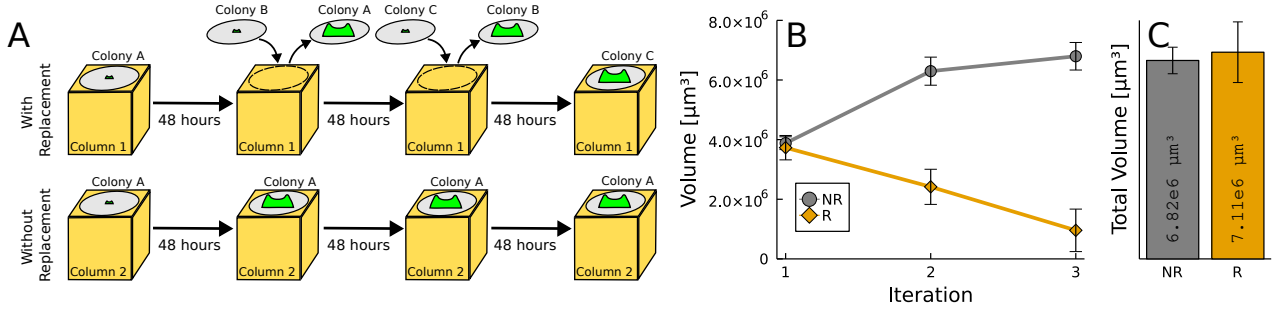

Figure S2. Growth of microbial colonies in a LB agar column, with (R) and without (NR) replacement every two days. (A) Descriptive cartoon for the experimental procedure. Colony profiles were measured after 48, 96 and 144 hours. The replacement step took less than 5 minutes from a fresh overnight. (B) Total amount of growth, in volume, for the columns with and without replacement. (C) Total cumulative growth, in volume for each column, for colonies without replacement (NR) it corresponds to the final volume, for columns with replacement (R) corresponds to the sum of the volume over the 3 iterations.

This experiment shows, as discussed in the main text, that a single column of LB agar can support more vertical growth than what would be obtained by a single colony reaching its steady state height. It is, nonetheless, interesting to note that the total growth volume, for colonies with and without replacement, is roughly the same (Figure S2). This is an interesting phenomenon, but it involves linking radial to volume growth, something that is out of the scope in the current study.

To accurately model the nutrient dynamics inside a biofilm colony, we have to incorporate the diffusion of the limiting nutrient through an interface. Given that our focus in this paper is in just, the vertical dynamics in the center region of the colony, we can model it as a 1-dimensional system:

$$\frac{\partial c}{\partial t} = D \cdot \frac{\partial^2 c}{\partial z^2} - \lambda \cdot \frac{c}{k+c} \tag{S1}$$

Where D is the diffusion coefficient, λ the consumption rate, and k the monod half-speed constant. The total growth rate in the colony, across the 1-dimensional space, can be approximated by a minimum function:

$$N(h, D, \lambda, k) = \int_0^h \frac{c(z)}{k + c(z)} dz \approx \min(h, L) \tag{S2}$$

The approximation from Equation S2 has a better agreement with the actual expression when k is small, as the Monod term $c/(k+c)$ will have a sharper transition (Figure S3).

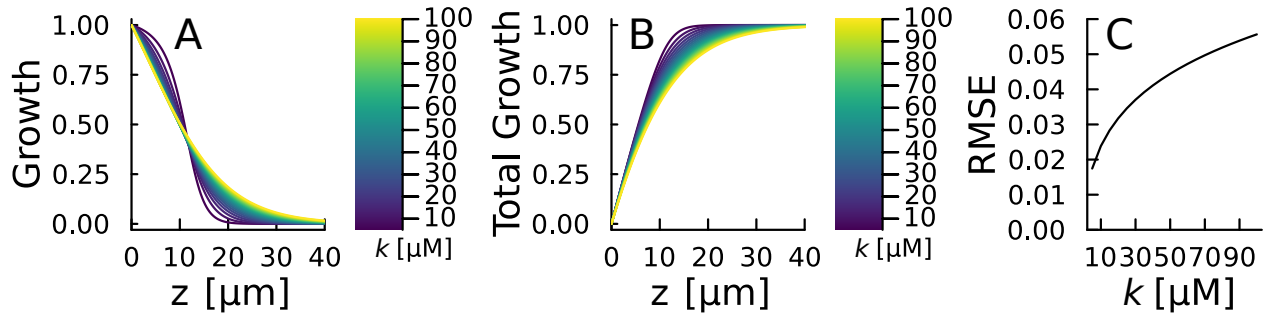

Figure S3. Nutrient dynamics. (A) Monod term $c/(k+c)$ for varying values of k in a 40 µm tall colony. (B) Total growth allowed in a colony, corresponding to the cumulative sum of panel A. (C) Root mean squared error between the actual numerical solution shown in panel B and the minimum function approximation.

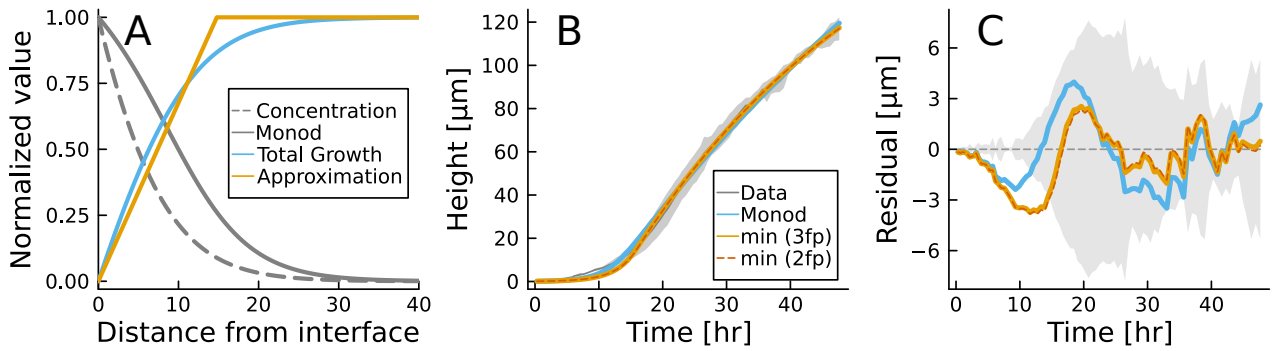

Figure S4. Test for the approximation of Equation S2 for L-serine consumption in a *E. coli* biofilm. (A) Nutrient dynamics after reaching equilibrium. The nutrient concentration profile (dashed gray) is plotted against the distance from the interface. The total allowed growth (light blue) is the cumulative of the monod term (solid gray). The approximation consists of a simple minimum function at the characteristic length L. (B) Best-fit models against experimental data. The numerically integrated Monod consumption (blue), the 3-parameter interface model with the approximation (orange), and interface model with the fixed best-fit value of L (dotted orange) all demonstrate good agreement with empirical data. (C) The residuals for the 3 models in comparison to the average and standard deviation values of 3 replicate colonies of *E. coli* over a period of 48 hours. The RMSE are 17.4, 15.68, and 15.75 μm respectively.

As determined by Croze et al. (1), the limiting nutrient for *Eschericia coli* in LB agar is the aminoacid L-serine. The corresponding values for the dynamics described by Equation S1 are $D = 800\mu m^2 \cdot s^{-1}$, $c_0 = 100\mu M$, $\lambda = 1.3 \cdot 10^3 \mu M \cdot s^{-1}$, $k = 38\mu M$. The height dynamics can be described then by:

$$\dot{h} = \alpha N(h, D, \lambda, k) - \beta h \tag{S3}$$

where α is the growth rate, $N(h, D, \lambda, k)$ the numerically integrated expression for growth, and β the decay rate. We test the results from this model, fitting α and β to our experimental data, as well as the validity of the approximation given by Equation S2 in Figure S4.
This shows that the approximation is good enough in a physiologically relevant regime for biofilms. Having good agreement when calculating the dynamics with 3 free parameters (yellow), and 2 free parameters with the best-fitted value of L (orange). The main advantage of this approximation relies on the simplification in the number of parameters: what was originally a function of the diffusion coefficient D, consumption rate λ, and Monod constant k is simplified to just an effective diffusion length L.

B. Model Comparisons

As an alternative to more complex models, incorporating multiple phases and spatial heterogeneities, we study the behavior of 3 simple models in addition to the proposed interface model, all describing the height dynamics of the biofilm colony $h(t)$. These reference models do not represent the state of the art, but instead provide a simple implementation of common modeling choices, allowing us to test their accuracy.
These 4 models (and their number of free parameters) are depicted in Figure S5, it is evident from the data that the Interface model has a better agreement both in the temporal dynamics and dependence on height across all sampled species.

Interface model (3). The model incorporates the nutrient dynamics in an implicit form, as described by Equation S2, leading to the formation of a finite-size growing layer and an increasing decay term.

$$\dot{h} = \alpha \cdot \min(h, L) - \beta \cdot h \tag{S4}$$

Where α is the growth rate, L the thickness of the active growing layer, and β the decay rate of the colony.

Logistic and nutrient depletion model (4). The model incorporates an auxiliary nutrient field that can get depleted locally, without incorporating diffusion through the vertical direction. Growth is also bounded to a carrying capacity.

$$\dot{h} = \alpha \cdot h \cdot \frac{c}{K_c + c} \cdot \left(1 - \frac{h}{K}\right) \qquad \dot{c} = -\epsilon \cdot \alpha \cdot h \cdot \frac{c}{K_c + c} \tag{S5}$$

Where c is the limiting nutrient concentration, α is the growth rate, K_c the Monod half-speed constant, K the carrying capacity for the biofilm, and ϵ an efficiency rate in the biomass transformation from nutrient to biofilm.

Logistic model (2). Growth is only constrained by a logistic carrying capacity, no dependence in nutrients.

$$\dot{h} = \alpha \cdot h \left(1 - \frac{h}{K}\right) \tag{S6}$$

Where c is the limiting nutrient concentration, α is the growth rate, and K the carrying capacity for the biofilm.

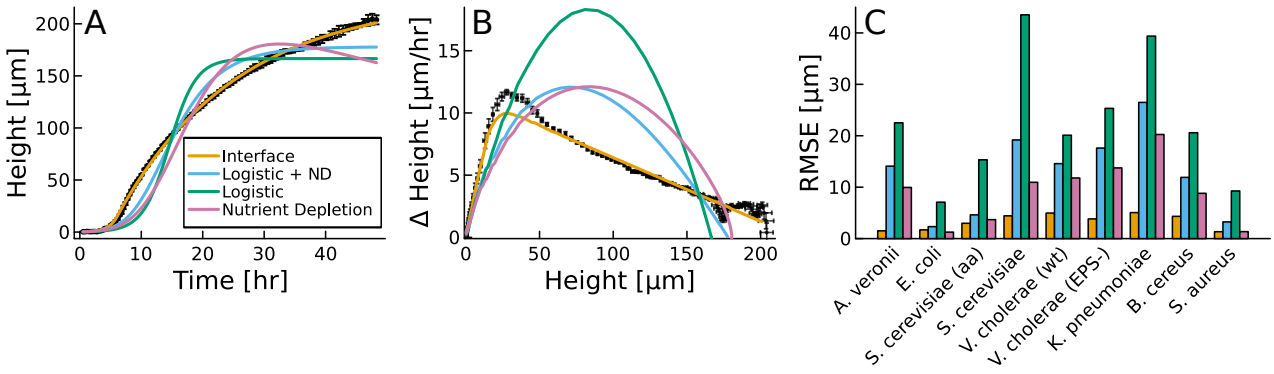

Figure S5. Interface and alternative models fitting to experimental height data across 48 hours. (A) Best-fit models for *A. veronii* across 48 hours. (B) Best-fit models in comparison to the two-regime behavior in *A. veronii*, alternative models are curved while the interface model has a sharp transition at $h = L$. (C) Root mean squared error for the best fit model in comparison to the experimental data for the 9 different strains of microbes tested in the study.

Nutrient depletion model (4). Growth depends linearly in the consumption of a nutrient field that cen get depleted locally, without incorporating its diffusion in the vertical direction. We also incorporate a decay term as in standard population dynamic models.

$$\dot{h} = \alpha \cdot h \cdot \frac{c}{K_c + c} - \beta h \qquad\qquad \dot{c} = -\epsilon \cdot \alpha \cdot h \cdot \frac{c}{K_c + c} \tag{S7}$$

Where c is the limiting nutrient concentration, α is the growth rate, K_c the Monod half-speed constant, β the decay rate, and ϵ an efficiency rate in the biomass transformation from nutrient to biofilm.

C. Long Time Behavior

We observe great quantitative agreement in the 48 hour range. However, the interface model also predicts the eventual saturation height, when the growth of the finite-size active layer equilibrates with the population-wide decay. This height is given by:

$$h_{\text{max}} = \frac{\alpha \cdot L}{\beta} \tag{S8}$$

We devised a long-time measurement experiment for 3 different microbes, with different growth and decay rates: (i) *A. veronii*, (ii) *E. coli*, and (iii) an aerotolerant anaerobic strain of *S. cerevisiae*. Reaching a height of 203.83 ± 4.34, 208.64 ± 8.07, and 116.88 ± 5.33 μm in the 48 hour range. Equation S8 predicts that *S. cerevisiae*, will continue to be the tallest colony by a considerable amount, and, more interestingly, that *E. coli* will surpass *A. veronii* in height, despite the fact that *A. veronii* is almost twice as tall as *E. coli* at 48 hours.

For this experiment, we inoculated 7 plates with 3 colonies each, and measured the height of the colonies every 2 days, for a period of 2 weeks. Each plate after measurement was discarded. This procedure was followed for each of the three strains.

Using the first 48 hours of growth and Equation S8, we bootstrap a distribution for h_{max}. We observe that for *A. veronii*, the height prediction and the actual best-fit value with the long-time data agree. For the two other strains, the prediction under-estimates the value of h_{max}, but remains within the 95 % confidence interval(Figure S6A).

The source of the range in height prediction is rooted in the difficulty of measuring β. β is small, on the order of 10 nm/hr. 48 hours is thus not necessarily enough time for an accurate measurement, leading to a wide range of effective growth rates at the end of the measurement. A colony that is already close to its steady state height (*A. veronii*) has a much narrower confidence interval than a colony that is still growing rapidly (*S. cerevisiae*). To determine β with narrow confidence intervals, a large amount of data in the $h > L$ regime is necessary.

To demonstrate this issue, we performed an 88 hour long timelapse of *E. coli*, and obtained the best fit parameters as a function of time. It is clear that by 40 hours α has already converged (Figure S6B), whereas β and L do not converge to their final values until $\sim$65 hours. It is important to note that the percentage change of these values varies greatly, with the limiting parameter being β, which at 50 hours is 230% of its final steady state value. On its own, fluctuations in β that range from 10-23 nm/hr do not seem substantial. However, in light of Equation S8, these fluctuations can greatly change the predicted final height of the colony. As a result, h_{max} cannot be accurately predicted until β is accurately measured.

D. Parameter estimation

We optimized all models (Equation S4, Equation S5, Equation S6, Equation S7) against experimental data with a sum of squared error loss J:

$$J(f(x), y) = \sum_{i}^{n} (f(x_i) - y_i)^2 \tag{S9}$$

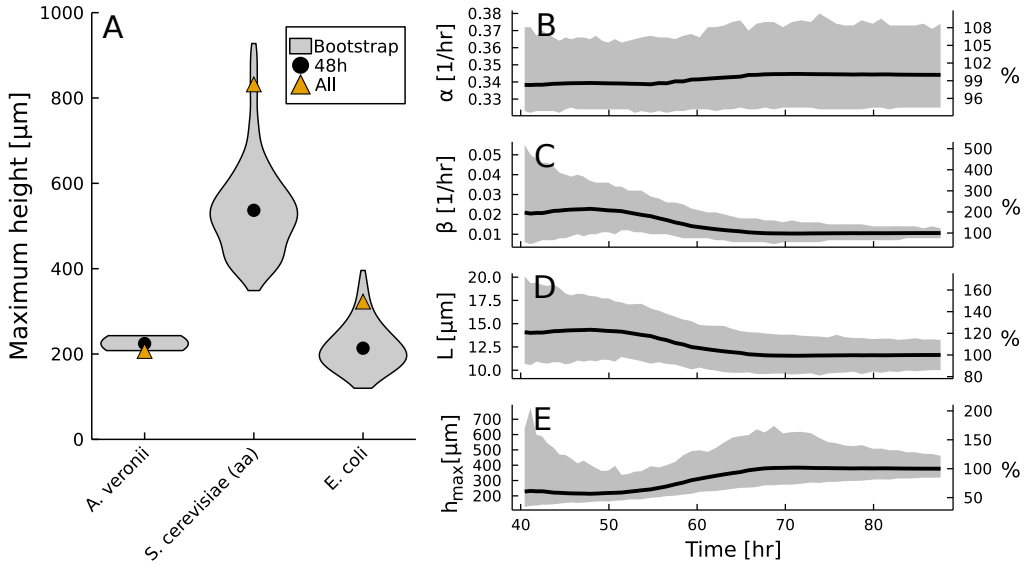

Figure S6. (A) Interface model h_{max} distributions after N=1000 bootstrapped fits are shown. Black circles represent the best fit for the initial 48 hour time period, and orange triangles represent the best fit including the measurements up to 14 days. (B-E) Best fit, and 90% confidence interval for the the three interface model parameters: α, β, L, and the steady state maximum height h_{max} are shown. On the left y-axis the actual values are reported, while on the right y-axis reports the value relative to the final 88 hour best fit value.

where y is the collection of experimental heights corresponding to measurement times t, $f(x)$ is the evaluation of the differential equation at time t. This allows us to directly compare the simulated predictions with our non equidistant temporal measurements. While this loss function J prioritizes better agreement with the data on higher heights, results do not suggest that compensating with higher weights at early times is needed since residual values are low across all the measurement period. To avoid any negative values in the fitting, we utilize a box-constrained optimization using the DifferentialEquations.jl(2) and DiffEqFlux.jl(3) packages. The limits for each parameters are detailed in Table S2.
For models containing an auxiliary nutrient field c, starting condition was set to $c_0 = 1.0$, with the needed scaling for the height dynamics being determined by ϵ.

Model	$\alpha[1/hr]$	$\beta[1/hr]$	$L[\mu m]$	$K[\mu m]$	$K_c[a.u.]$	ϵ
Interface	$[10^{-5}, 10^{3}]$	$[10^{-5}, 10^{2}]$	$[1, 10^{5}]$	-	-	-
Logistic + Nutrient depletion	$[10^{-5}, 10^{3}]$	-	-	$[1, 10^{5}]$	$[10^{-5}, 10^{3}]$	$[10^{-5}, 10^{5}]$
Logistic	$[10^{-5}, 10^{3}]$	-	-	$[1, 10^{5}]$	-	-
Nutrient depletion	$[10^{-5}, 10^{3}]$	$[10^{-5}, 10^{2}]$	-	-	$[10^{-5}, 10^{3}]$	$[10^{-5}, 10^{5}]$

Table S2. Fitting boundaries for model fitting. Ranges push the boundaries of what makes physical/biological sense by at least an order of magnitude.

To get confidence intervals and parameter distributions we utilize a moving block bootstrap across the 3 different replicates, sampling n=20 blocks of size s=5, returning a total of 100 points, roughly the same amount as an individual timelapse. We iterate for i=1:1000 times and obtain the best-fit parameters α_i, β_i, L_i. Then utilizing Equation S8, discard the outlying 5% values.

Bibliography

1. OA Croze, GP Ferguson, ME Cates, WC Poon, Migration of chemotactic bacteria in soft agar: role of gel concentration. *Biophysical journal* **101**, 525–534 (2011).
2. C Rackauckas, Q Nie, DifferentialEquations.jl – A Performant and Feature-Rich Ecosystem for Solving Differential Equations in Julia. *Journal of Open Research Software* **5**, 15 (2017) Number: 1 Publisher: Ubiquity Press.
3. C Rackauckas, et al., Universal differential equations for scientific machine learning. *arXiv preprint arXiv:2001.04385* (2020).

Supplementary Videos

Figure SV1. This is a video of a lysosome.
A typical caption would go here. We use a thumbnail version of the video file as the figure.
Time, seconds. Scale bar, 10 µm.